Chemical Science

EDGE ARTICLE

View Article Online
View Journal | View Issue

Cite this: *Chem. Sci.*, 2014, **5**, 156

# Conversion of high-spin iron(III)–alkylperoxo to iron(IV)–oxo species *via* O–O bond homolysis in nonheme iron models†

Seungwoo Hong,‡[ab] Yong-Min Lee,‡[a] Kyung-Bin Cho,[a] Mi Sook Seo,[a] Dayoung Song,[a] Jihae Yoon,[a] Ricardo Garcia-Serres,[c] Martin Clémancey,[d] Takashi Ogura,[e] Woonsup Shin,*[b] Jean-Marc Latour*[f] and Wonwoo Nam*[a]

The mechanism of the alkylperoxo O–O bond cleavage of low-spin iron(III)–alkylperoxo species has been well established in nonheme iron models. In contrast, the alkylperoxo O–O bond cleavage in nonheme high-spin iron(III)–alkylperoxo species binding an axial ligand has yet to be elucidated. Herein, we report the synthesis and characterization of mononuclear nonheme high-spin iron(III)–alkylperoxo complexes each bearing an *N*-tetramethylated 13-membered macrocyclic ligand (13-TMC), $[Fe^{III}(OOC(CH_3)_3)$-(13-TMC)]$^{2+}$ and $[Fe^{III}(OOC(CH_3)_2C_6H_5)$(13-TMC)]$^{2+}$. The high-spin iron(III)–alkylperoxo complexes were converted to an iron(IV)–oxo complex at a fast rate upon addition of thiocyanate ($NCS^-$) *via* the formation of a short-lived intermediate. This intermediate was identified as a high-spin iron(III)–alkylperoxo complex binding a thiocyanate ion as an axial ligand by characterizing it with various spectroscopic methods and density functional theory (DFT) calculations. We have also provided strong evidence that conversion of the high-spin iron(III)–alkylperoxo complex to its corresponding iron(IV)–oxo complex occurs *via* O–O bond homolysis. Thus, we have concluded that the role of the axial ligand binding to a high-spin iron(III)–alkylperoxo complex is to facilitate the alkylperoxo O–O bond cleavage *via* the "push effect", which has been well established in heme enzymes. To the best of our knowledge, the present study reports the first clear example showing the O–O bond homolysis of a high-spin iron(III)–alkylperoxo complex and the axial ligand effect on the alkylperoxo O–O bond cleavage in nonheme iron models.

Received 9th August 2013
Accepted 17th September 2013

DOI: 10.1039/c3sc52236a

www.rsc.org/chemicalscience



## Introduction

Iron–dioxygen adducts, including iron(III)–hydroperoxo ($Fe^{III}$–OOH) and iron(III)–alkylperoxo ($Fe^{III}$–$OOCR_3$) species, have been identified as key intermediates in the catalytic cycles of dioxygen activation by heme and nonheme iron enzymes.[1–3] The peroxide ligands of the iron(III)–hydroperoxo and –alkylperoxo species are cleaved either homolytically or heterolytically, resulting in the generation of high-valent iron(IV or V)–oxo intermediates as active oxidants that affect the oxidation of organic substrates. A notable example is the formation of the iron(IV)–oxo porphyrin π-cation radical species, referred to as Compound I (Cpd I), *via* heterolytic O–O bond cleavage of

[a]*Department of Chemistry and Nano Science, Department of Bioinspired Science, Center for Biomimetic System, Ewha Womans University, Seoul 120-750, Korea. E-mail: wwnam@ewha.ac.kr*

[b]*Department of Chemistry and Interdisciplinary Program of Integrated Biotechnology, Sogang University, Seoul 121-742, Korea. E-mail: shinws@sogang.ac.kr*

[c]*University of Grenoble Alpes, LCBM, F-38054 Grenoble, France*

[d]*CNRS UMR 5249, LCBM, F-38054 Grenoble, France*

[e]*Picobiology Institute, Graduate School of Life Science, University of Hyogo, Hyogo 678-1297, Japan*

[f]*CEA, DSV, iRTSV, LCBM, PMB, F-38054 Grenoble, France. E-mail: jean-marc.latour@cea.fr*

† Electronic supplementary information (ESI) available: Experimental section; synthesis, characterization, kinetics and DFT details. CCDC reference number 959085. For ESI and crystallographic data in CIF or other electronic format see DOI: 10.1039/c3sc52236a

‡ These authors contributed equally to this work.

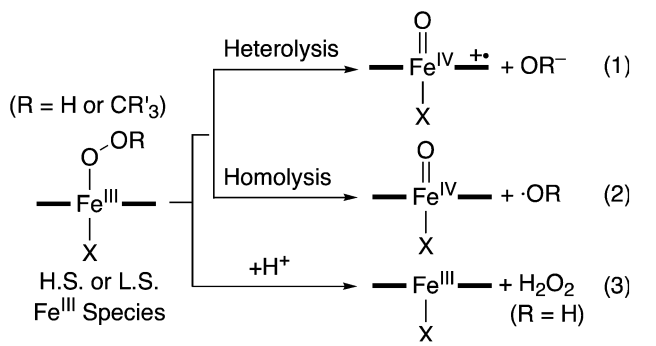


Scheme 1

iron(III)–hydroperoxo intermediates in cytochromes P450 and their models (Scheme 1, eqn (1)).[2] In the case of nonheme iron models, the formation of iron(IV)–oxo complexes *via* the O–O bond homolysis of iron(III)–hydroperoxo and –alkylperoxo species has been reported with spectroscopic evidence (Scheme 1, eqn (2)).[4] Similarly, the homolytic O–O bond cleavage of nonheme manganese(III)–alkylperoxo complexes has been demonstrated recently.[5] In addition to the peroxide O–O bond cleavage, iron(III)–hydroperoxo species undergo a protonation-assisted loss of $H_2O_2$ *via* Fe–O bond cleavage (Scheme 1, eqn (3)). One example in nonheme iron enzymes is superoxide reductase (SOR), which reduces superoxide to hydrogen peroxide as part of the organism's natural defenses in anaerobic and microaerophilic organisms.[6–8]

It has been well documented that the fate of the peroxide ligands of the Fe(III)–OOR(H) species is markedly affected by axial ligands in enzymatic and biomimetic reactions (*e.g.*, heterolytic and homolytic O–O bond cleavage and $H_2O_2$ release as shown in Scheme 1).[2,9] Spin states of the Fe(III)–OOR(H) species (*e.g.*, high-spin (H.S.) and low-spin (L.S.) iron(III) ions) have also been considered as an important factor that modulates the strength of Fe–O and O–O bonds, thereby determining the reaction pathways such as the O–O bond *vs* Fe–O bond cleavage of nonheme Fe(III)–OOR(H) species (Scheme 1).[10] For example, it has been shown that low-spin iron(III)–alkylperoxo complexes undergo homolytic O–O cleavage of the alkylperoxide ligands to form iron(IV)–oxo species (Scheme 1, eqn (2)),[4b,10a] whereas Fe–O bond cleavage occurs preferentially in high-spin iron(III)–alkylperoxo species (Scheme 1, eqn (3)).[8b,c,9b] However, the axial ligand effect on the O–O bond or Fe–O bond cleavage in high-spin iron(III)–alkylperoxo species has yet to be elucidated, although a number of high-spin iron(III)–alkylperoxo complexes have been synthesized and characterized well.[8,11] Herein, we report the synthesis and characterization of mononuclear nonheme high-spin iron(III)–alkylperoxo complexes each bearing an *N*-tetramethylated 13-membered macrocyclic ligand (13-TMC = 1,4,7,10-tetramethyl-1,4,7,10-tetraazacyclotridecane).[12] This high-spin iron(III)–alkylperoxo complex is converted to the corresponding iron(IV)–oxo complex upon binding of an anionic ligand. The iron(IV)–oxo product with the anionic axial ligand is fully characterized with various spectroscopic methods. The mechanism of the O–O bond cleavage of the high-spin iron(III)–alkylperoxo complex upon binding an anionic axial ligand is discussed as well.

## Results and discussion

The starting iron(II) complex, $Fe^{II}$(13-TMC)$(CF_3SO_3)_2$ (**1**), was synthesized by reacting equimolar amounts of $Fe^{II}(CF_3SO_3)_2$ and 13-TMC in $CH_3CN$ under an inert atmosphere, as reported previously.[13] Addition of alkyl hydroperoxides, such as *tert*-butyl hydroperoxide (*t*-BuOOH) and cumyl hydroperoxide (Cumyl-OOH), to **1** in $CH_3CN$ at −40 °C afforded the formation of purple intermediates, denoted as $^{BH}$**2** and $^{CH}$**2**, respectively. The intermediates were metastable ($t_{1/2}$ ∼ 1.5 h) under the reaction conditions and characterized with various spectroscopic methods, including UV-vis, electron paramagnetic resonance (EPR), Mössbauer, and resonance Raman (rRaman) spectroscopies.

The UV-vis spectra of $^{BH}$**2** and $^{CH}$**2** exhibit maximum absorption bands at 510 nm ($\varepsilon$ = 1100 $M^{-1}$ $cm^{-1}$) and 500 nm ($\varepsilon$ = 1000 $M^{-1}$ $cm^{-1}$) (Fig. 1a for $^{BH}$**2** and ESI, Fig. S1† for $^{CH}$**2**), respectively; these bands are assigned to an alkylperoxo-to-iron(III) charge transfer band (LMCT).[8,11] The X-band EPR spectra of $^{BH}$**2** and $^{CH}$**2**, recorded in a frozen $CH_3CN$ solution at 5 K, exhibit signals corresponding to high-spin ($S$ = 5/2) iron(III) species with $g$ values of 6.8, 5.4, and 2.0 for $^{BH}$**2** and 6.3, 5.5, and 2.1 for $^{CH}$**2** (ESI, Fig. S2†).[8c,11b,c] The Mössbauer spectrum of $^{BH}$**2**, recorded at 4.2 K (Fig. 2a) in the absence of a strong applied magnetic field, displays a central doublet and a broad magnetic component, which can be interpreted as a single high-spin ferric species in two differing relaxation states (ESI, Fig. S3 and S4† for **1** and $^{BH}$**2**, respectively). A small amount of unreacted **1** (8%, green line) is also present. The spectrum is difficult to simulate due to a distribution of internal fields. However, this distribution can be lifted by the application of a 7 T magnetic field that aligns the magnetic moments, giving rise to the six-line spectrum displayed in Fig. 2b, characteristic of a high-spin ferric ion. Most of the spectrum (∼90% of the absorption) could be simulated with parameters consistent with this assignment (ESI, Table S1†). It is noteworthy that this species possesses a large zero-field splitting in the range of those of high-spin ferric hemes and a small isomer shift more in line with a low-spin $Fe^{III}$. However, attempts to simulate it as an $S$ = 1/2 system were unsuccessful.

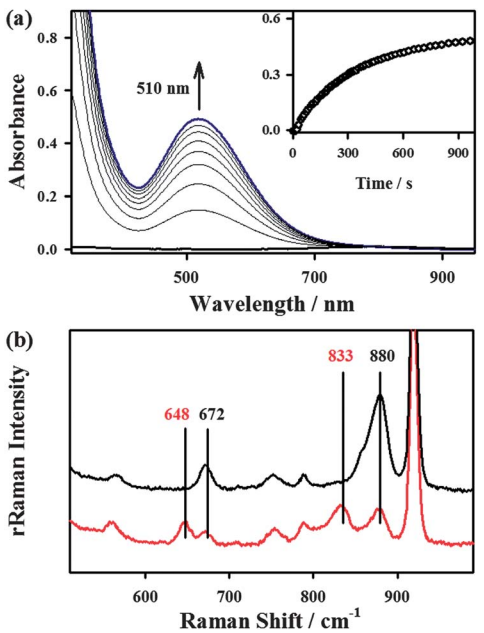


Fig. 1 (a) UV-vis spectrum of $^{BH}$**2** formed in the reaction of **1** (0.50 mM) and *t*-BuOOH (1.5 mM) in $CH_3CN$ at −40 °C. Inset shows the time trace monitored at 510 nm for the formation of $^{BH}$**2**. (b) Resonance Raman spectra of [(13-TMC)$Fe^{III}(^{16}O^{16}O$Cumyl)]$^{2+}$ (black line) and [(13-TMC)$Fe^{III}(^{18}O^{18}O$Cumyl)]$^{2+}$ (red line) generated in the reactions of **1** (16 mM) and 3 equiv. of Cumyl-$^{16}O^{16}$OH and Cumyl-$^{18}O^{18}$OH (70% $^{18}$O enriched), respectively, in $CH_3CN$ at −40 °C ($\lambda_{ex}$ = 442 nm).

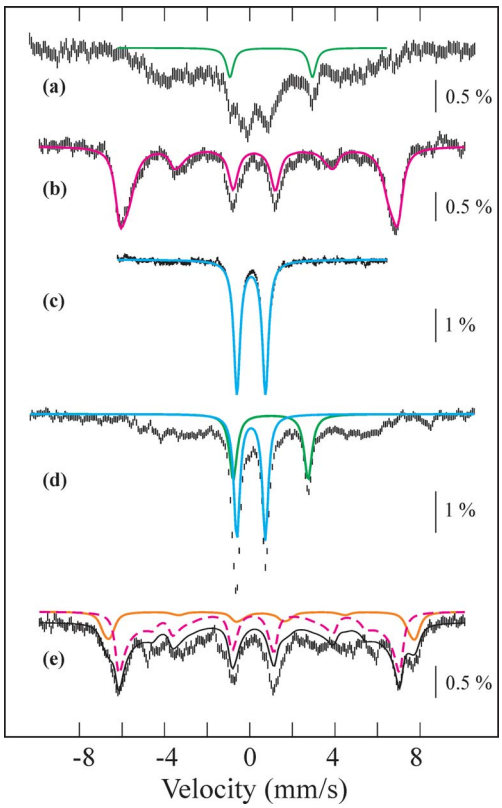


Fig. 2 Mössbauer spectra of intermediates formed in the reactions of **1** and *t*-BuOOH before (a and b) after (d and e) addition of $NCS^-$, and an authentic compound **4** (c). Data was collected at 4.2 K in a parallel applied field of 0.06 T (a, c, and d) or 7 T (b and e). The colored lines represent theoretical simulations of individual species $Fe^{II}$ (green), $^{BH}$**2** (pink), **4** (blue), and **3** (pink-dashed). The orange component is an impurity. The Mössbauer and zero-field splitting parameters used in the simulations are listed in ESI, Table S1.† They are derived from the applied-field studies represented in ESI, Fig. S4, S7, and S8.†

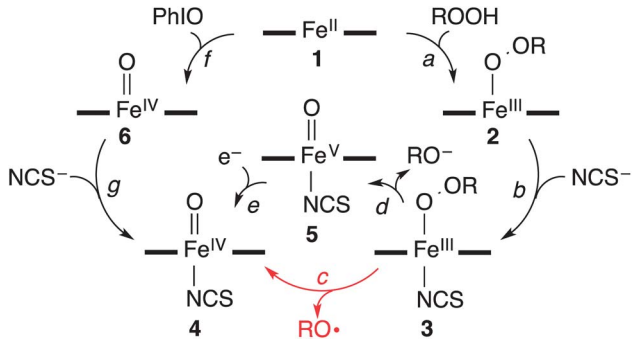


Scheme 2

The rRaman spectrum of $^{CH}$**2**, obtained upon 442 nm excitation in $CH_3CN$ at −40 °C, shows two isotopically sensitive bands at 672 and 880 $cm^{-1}$ (Fig. 1b). The peak at 672 $cm^{-1}$ shifts to 648 $cm^{-1}$ upon $^{18}$O-substitution with a $^{16,18}\Delta$ value of 24 $cm^{-1}$ and is assigned to the Fe–O stretch.[14] The peak at 880 $cm^{-1}$ shifts to 833 $cm^{-1}$ upon $^{18}$O-substitution with a $^{16,18}\Delta$ = 47 $cm^{-1}$ and is the O–O stretch.[14] One notable observation in the rRaman data is that the Fe–O stretch of $^{CH}$**2** is higher than those of the previously reported high-spin Fe(III)–OOR complexes (*e.g.*, $\nu_{Fe-O}$ of 612 $cm^{-1}$ for $[Fe^{III}(OOC(CH_3)_3)(15\text{-TMC})(OTf)]^+$; 15-TMC = 1,4,8,12-tetramethyl-1,4,8,12-tetraazacyclopentadecane, $OTf^-$ = $CF_3SO_3^-$),[8c,11] indicating that this high-spin iron(III)–alkylperoxo complex possesses a stronger Fe–O bond. Based on the spectroscopic characterization of the $^{BH}$**2** and $^{CH}$**2** intermediates, we conclude that high-spin iron(III)–alkylperoxo complexes, assigned as $[Fe^{III}(OOC(CH_3)_3)(13\text{-TMC})]^{2+}$ for $^{BH}$**2** and $[Fe^{III}(OOC(CH_3)_2C_6H_5)(13\text{-TMC})]^{2+}$ for $^{CH}$**2**, were produced in the reactions of **1** and alkyl hydroperoxides (Scheme 2, reaction a).

Interestingly, the addition of 1.2 equiv. of thiocyanate ($NCS^-$) to the solutions of $^{BH}$**2** and $^{CH}$**2** yielded a green intermediate **4** with a broad electronic absorption band at 755 nm (Fig. 3 and ESI, S5†). The full conversion of $^{BH}$**2** to **4** was found to require one equiv. of thiocyanate by carrying out a titration experiment (Fig. 3, inset). The intermediate **4** with a characteristic absorption band of nonheme iron(IV)–oxo complexes[15,16] was assigned unequivocally as $[Fe^{IV}(O)(13\text{-TMC})(NCS)]^+$ (Scheme 2, structure **4**) by characterizing it with various spectroscopic methods and comparing the spectroscopic data with those of an authentic iron(IV)–oxo compound prepared independently (*vide infra*).

The authentic compound, $[Fe^{IV}(O)(13\text{-TMC})(NCS)]^+$ (**4**), was synthesized as follows: the reaction of **1** with 3 equiv. of iodosylbenzene (PhIO) in $CH_3CN$ at −40 °C afforded a green intermediate which was identified as $[Fe^{IV}(O)(13\text{-TMC})]^{2+}$ (**6**), as reported previously (Scheme 2, reaction f) (See ESI, Fig. S6† for the electrospray ionization mass spectrometry (ESI MS), UV-vis, and rRaman spectroscopy).[13] The authentic compound **4** was then prepared by adding 1.2 equiv. of $NCS^-$ to the solution of **6** in $CH_3CN$ at −40 °C (Scheme 2, reaction g), by following literature methods for the synthesis of axial ligand-substituted $[Fe^{IV}(O)(14\text{-TMC})(X)]^+$ complexes (14-TMC = 1,4,8,11-tetramethyl-1,4,8,11-tetraazacyclotetradecane; $X^-$ = $NCS^-$ and $N_3^-$).[15,17] The authentic

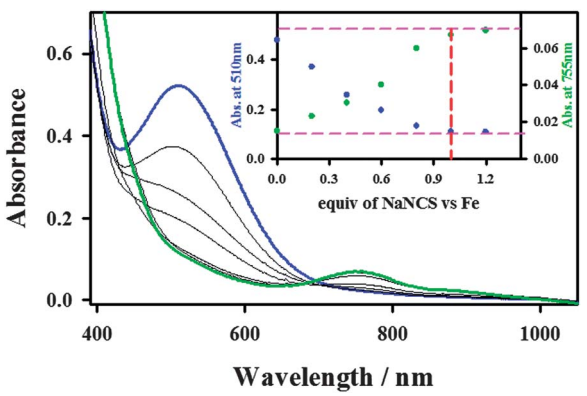


Fig. 3 UV-vis spectral changes showing the conversion of $^{BH}$**2** (blue, 0.50 mM) to **4** (green) with respect to the amount of thiocyanate added (0.20, 0.40, 0.60, 0.80, 1.0, and 1.2 equiv.) in $CH_3CN$ at −40 °C. Inset shows the absorbance recorded at 510 nm (blue circle) and 755 nm (green circle). Two horizontal dashed pink lines and one vertical dashed red line indicate the two saturation values and 1.0 equiv. of $NCS^-$ added, respectively.

compound **4** was characterized with UV-vis, ESI MS, rRaman, and Mössbauer, and the spectroscopic data of the authentic compound **4** were compared with those of the product **4** formed in the reaction of $^{BH}$**2** and $NCS^-$. The UV-vis spectrum of **4** exhibits an absorption band at $\lambda_{max} = 755$ nm ($\varepsilon = 160\ M^{-1}\ cm^{-1}$) (ESI, Fig. S9a†). The ESI MS of **4** exhibits a prominent ion peak at a mass-to-charge ($m/z$) ratio of 372.2 (Fig. S9b†), whose mass and isotope distribution pattern correspond to $[Fe^{IV}(O)(13\text{-TMC})(NCS)]^+$ (calculated $m/z$ 372.2). When **4** was prepared with isotopically labeled $PhI^{18}O$ in the presence of $H_2{}^{18}O$, the mass peak corresponding to **4** shifted to $m/z$ 374.2 (Fig. S9b,† inset), indicating that **4** contains an oxygen atom. The rRaman spectrum of **4**, obtained upon 407 nm excitation in $CH_3CN$ at −40 °C, exhibits an isotope-sensitive band at 848 $cm^{-1}$, which shifted to 810 $cm^{-1}$ when **4**-$^{18}$O was generated with isotopically labeled $PhI^{18}O$ in the presence of a small amount of $H_2{}^{18}O$ in $CH_3CN$ (Fig. S9c†). The observed isotopic shift of −38 $cm^{-1}$ with $^{18}$O-substitution is in agreement with the calculated value ($\Delta\nu_{calc} = -37\ cm^{-1}$) for an Fe–O diatomic vibration. Thus, the peak at 848 $cm^{-1}$ is assigned to the Fe–O stretch, as reported in mononuclear nonheme iron(IV)–oxo complexes bearing 14-TMC and N4Py ligands (N4Py = *N*,*N*-bis(2-pyridylmethyl)-*N*-bis(2-pyridyl)methylamine).[15a,c,16] The low-field Mössbauer spectrum of **4** recorded at 4.2 K (Fig. 2c) consists of a quadrupole doublet with $\delta = 0.07$ mm $s^{-1}$ and $\Delta E_Q = 1.34$ mm $s^{-1}$, characteristic of an $S = 1$ $Fe^{IV}$=O species.[16] The $S = 1$ ground state was confirmed by a high-field experiment (ESI, Fig. S10†). The Mössbauer parameters used in the simulation are listed in ESI, Table S1.† Based on the spectroscopic characterization of **4**, we are able to confirm unambiguously that **4** is an iron(IV)–oxo complex binding an anionic axial ligand ($NCS^-$), $[Fe^{IV}(O)(13\text{-TMC})(NCS)]^+$. We therefore conclude that addition of an anionic ligand to high-spin iron(III)–alkylperoxo complexes (**2**) afforded the formation of an iron(IV)–oxo complex (**4**) (Scheme 2, reaction b) (*vide infra*).

Since the conversion of **2** to **4** was too fast to follow the reaction with a UV-vis spectrophotometer (ESI, Fig. S5†), the reaction of **2** with $NCS^-$ was investigated with stopped-flow spectrophotometry. As shown in Fig. 4, addition of $NCS^-$ to the solution of $^{BH}$**2** in $CH_3CN$ at −40 °C generated a new intermediate **3** with an absorption band at 458 nm within 0.1 s, which was then fully converted to **4** within 40 s. The characterization of the new intermediate **3** was attempted spectroscopically despite its short lifetime. The X-band EPR spectra of **3**, which was prepared by reacting $^{BH}$**2** and $NCS^-$ in $CH_3CN$ at −40 °C and frozen immediately at the given times, exhibit signals corresponding to high-spin iron(III) species (Fig. 4c); the signal intensities were low due to its fast conversion to an EPR inactive iron(IV)–oxo species. It should also be noted that signals corresponding to low-spin iron(III) species were not observed in the EPR measurements (Fig. 4c). The Mössbauer spectra of **3** recorded at 4.2 K in a parallel applied field of 600 G or 7 T are depicted in Fig. 2. The weak field spectrum (Fig. 2d) shows the presence of two minor doublets and a major broad magnetic component. The two doublets are associated with an $Fe^{II}$ (15% of total iron, green line) and an $Fe^{IV}$=O (20% of total iron, blue line) species as judged from their parameters (ESI, Table S1†). The parameters of the $Fe^{IV}$ doublet are identical to those of

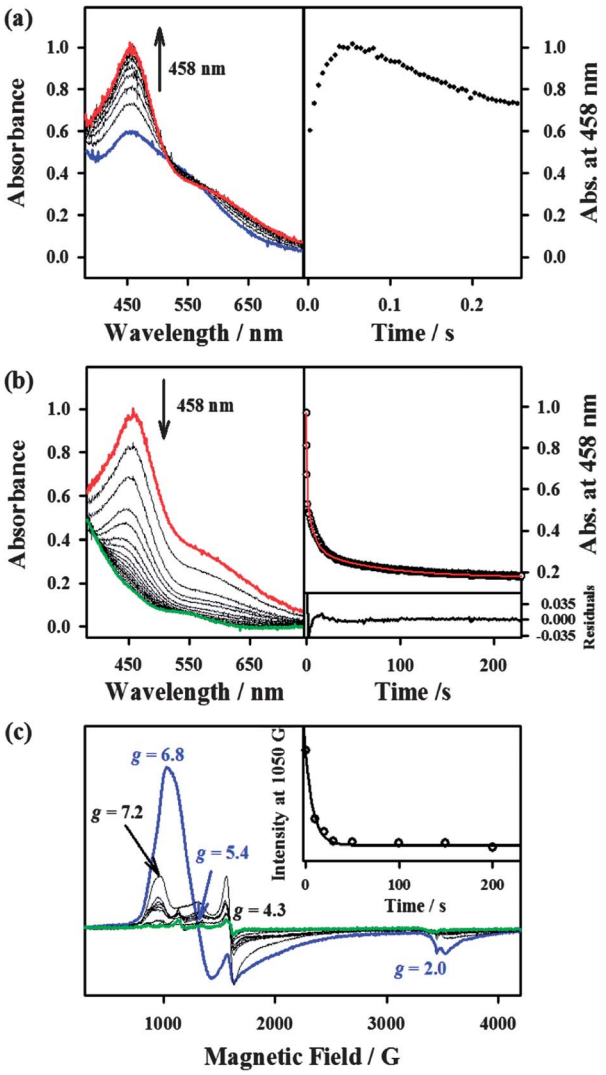


Fig. 4 Spectral changes and time courses obtained in the reactions of $^{BH}$**2** (0.50 mM) with thiocyanate (0.60 mM), using single-mixing stopped-flow spectrophotometry and monitoring the formation of the presumed $^{BH}$**2-NCS** (**3**) intermediate at 458 nm in $CH_3CN$ at −40 °C. (a) UV-vis spectral changes (left) and time trace (right) recorded during the formation of $^{BH}$**2-NCS** (200 ms). (b) UV-vis spectral changes (left) and time trace (upper right) recorded during the decay of $^{BH}$**2-NCS** (300 s). (c) X-band EPR spectral changes of $^{BH}$**2** (0.50 mM) (blue) upon the addition of thiocyanate (0.60 mM). The spectra were taken at 0, 10, 20, 30, 50, 100, 150, 200, and 300 s after $NCS^-$ was added in $CH_3CN$ at −40 °C. $^{BH}$**2-NCS** (black) with $g = 7.2$, 4.3 was formed upon addition of $NCS^-$. The final spectrum is shown with a green line. Inset shows the time dependence of the EPR signal intensity at 1050 G.

genuine **4**, but those of the $Fe^{II}$ doublet ($\delta = 0.98$ mm $s^{-1}$, $\Delta E_Q = 3.15$ mm $s^{-1}$) are not the same as those of **1**, indicating a difference in the iron coordination sphere.[18] Such a difference could result from the substitution of a $CH_3CN$ ligand for an $NCS^-$ ligand. Fig. 2e shows the spectrum recorded at 7 T after subtraction of the $Fe^{IV}$=O species. The spectrum is very similar to that of $^{BH}$**2**, although the highest velocity line is split in two, revealing the presence of two high-spin ferric species. The spectrum can be fitted with two high-spin $Fe^{III}$ components, one accounting for 13% of total iron with parameters that are

common for octahedral high-spin $Fe^{III}$ (orange line), and a majority species (42% of total iron, pink line) with atypical parameters (ESI, Fig. S11 and Table S1†) similar to those of $^{BH}$**2**, but with an even larger zero-field splitting value. Owing to its peculiar parameters similar to but distinct from those of $^{BH}$**2**, the latter component is assigned to **3**, and the former component with classical parameters is assigned to a degradation product.

The structure of **3** was further corroborated with density functional theory (DFT) calculations.[19,20] First, the structure of the DFT-optimized $^{BH}$**2** is shown in Fig. 5a. The energetically lowest structure is in agreement with the high-spin iron(III) state determined in experiments; 9.3 kcal $mol^{-1}$ lower than the $S = 3/2$ intermediate-spin state and 16.4 kcal $mol^{-1}$ lower than the $S = 1/2$ low-spin state. Addition of $NCS^-$ to this structure to form **3** (Fig. 5b) significantly lowers the $S = 1/2$ low-spin state closer to the ground state on an electron energy level, 0.4 kcal $mol^{-1}$ higher than the $S = 5/2$ high-spin state. However, including zero-point vibrational energies (and other correction factors) and looking at the free energy (see ESI, DFT methods description and Table S4†), the $S = 5/2$ high-spin state is likely to be even more stable than this. Hence, we consider that the DFT-optimized structure of **3** is in agreement with experiments. Based on the EPR and Mössbauer spectroscopic analysis and the DFT-optimized structure, we propose that **3** is a high-spin iron(III)–alkylperoxo complex binding an anionic axial ligand, $[Fe^{III}(OOC(CH_3)_3)(13\text{-TMC})(NCS)]^+$ (**3**),[21] which is rapidly converted to **4** *via* O–O bond cleavage (*vide infra*).

Then, how is the O–O bond of the alkylperoxide of **3** cleaved to form **4**? Two possible mechanisms are considered, namely O–O bond homolysis (Scheme 2, reaction c) and O–O bond heterolysis followed by a one electron reduction (Scheme 2, reactions d and e). Since cumyl hydroperoxide is a well-known mechanistic probe that can be used to distinguish homolytic *vs* heterolytic O–O bond cleaving pathways,[5b,22] the products formed in the reaction solution were analyzed. The product analysis revealed the exclusive formation of acetophenone (~80% based on the amount of the intermediate $^{CH}$**2**) (Scheme 3, pathway a), as opposed to cumyl alcohol (0%)

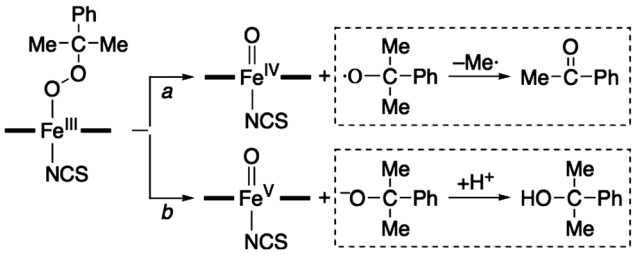


Scheme 3

(Scheme 3, pathway b) (ESI, Experimental section†). The observation of the acetophenone formation as the sole product demonstrates that the conversion of **3** to **4** occurs exclusively *via* O–O bond homolysis (Scheme 2, reaction c highlighted with a red color), not *via* O–O bond heterolysis followed by a one electron reduction (Scheme 2, reactions d and e). As a conclusion, we have shown here that the binding of an anionic axial ligand by a high-spin iron(III)–alkylperoxo complex bearing an *N*-tetramethylated macrocyclic ligand facilitates O–O bond cleavage *via* the "push effect", which has been well established in heme enzymes (*e.g.*, CYP 450 and peroxidases) and their model reactions.[23,24] We have also shown that O–O bond cleavage of a high-spin iron(III)–alkylperoxo complex binding an anionic axial ligand occurs homolytically, resulting in the generation of its corresponding iron(IV)–oxo complex (Scheme 2, reactions b and c).

## Conclusion

We have reported the synthesis and characterization of high-spin iron(III)–alkylperoxo complexes each bearing a macrocyclic ligand. The intermediates are stable at low temperature, but are converted to an iron(IV)–oxo complex rapidly upon binding of an anionic axial ligand. We have also provided strong evidence that the conversion of the high-spin iron(III)–alkylperoxo complexes to the iron(IV)–oxo species occurs *via* O–O bond homolysis. These observations imply that binding of an anionic axial ligand by high-spin iron(III)–alkylperoxo species facilitates O–O bond cleavage, not Fe–O bond cleavage, and that the O–O bond cleavage occurs *via* a homolytic O–O cleavage mechanism. These results are in sharp contrast to those reported previously which showed that nonheme high-spin iron(III)–alkylperoxo complexes possess weak Fe–O and strong O–O bonds that give rise to Fe–O bond homolysis rather than O–O bond cleavage.[8,9a,10b] Further, it should be noted that the present results are different from the previously proposed role of the thiolate axial ligand *trans* to the iron-hydroperoxo moiety in SOR and its model compounds, *i.e.* that the electron-donating thiolate ligand increases the lifetime of the high-spin iron(III)–hydroperoxo species to allow its protonation and subsequent release of $H_2O_2$ in SOR.[7a,11d,25] Further mechanistic investigation, including DFT calculations, is underway in this laboratory to understand the factors (*e.g.*, effects of the axial ligand and the H.S. and L.S. iron(III) spin states) that affect the activation of iron(III)–alkylperoxo and –hydroperoxo complexes in nonheme iron models.[26]

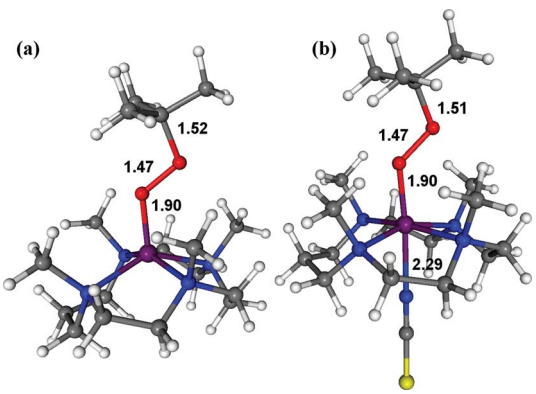


Fig. 5 DFT-calculated structures of $^{BH}$**2** (a) and **3** (b). The O–C, O–O, O–Fe, and Fe–NCS bond lengths are indicated in Å (Fe, purple; N, blue; O, red; C, grey; S, yellow; H, white).

## Acknowledgements

The research at EWU was supported by NRF/MEST of Korea through the CRI (2-2012-1794-001-1 to W.N.), GRL (2010-00353 to W.N.), and Basic Research Program (2010-0002558 to M.S.S.). J.M.L. acknowledges the support of the Region Rhone-Alpes through contract CIBLE 07 016335 and Labex ARCANE (ANR-11-LABX-0003-01). T.O. thanks the Ministry of Education, Culture, Sports, Science and Technology of Japan through the Global COE program and Priority Area (no. 22018026).

## Notes and references

1 W. Nam, *Acc. Chem. Res.*, 2007, **40**, 465, and review articles in the special issue.

2 (*a*) P. R. Ortiz de Montellano in *Cytochrome P450: Structure, Mechanism, and Biochemistry*, Kluwer Academic/Plenum Publishers, New York, 2005; (*b*) P. R. Ortiz de Montellano, *Chem. Rev.*, 2010, **110**, 932–948; (*c*) S. Shaik, S. Cohen, Y. Wang, H. Chen, D. Kumar and W. Thiel, *Chem. Rev.*, 2010, **110**, 949–1017; (*d*) J. Rittle and M. T. Green, *Science*, 2010, **330**, 933–937.

3 (*a*) E. G. Kovaleva and J. D. Lipscomb, *Nat. Chem. Biol.*, 2008, **4**, 186–193; (*b*) E. I. Solomon, S. D. Wong, L. V. Liu, A. Decker and M. S. Chow, *Curr. Opin. Chem. Biol.*, 2009, **13**, 99–113.

4 (*a*) J. Cho, S. Jeon, S. A. Wilson, L. V. Liu, E. A. Kang, J. J. Braymer, M. H. Lim, B. Hedman, K. O. Hodgson, J. S. Valentine, E. I. Solomon and W. Nam, *Nature*, 2011, **478**, 502–505; (*b*) J. Kaizer, M. Costas and L. Que, Jr, *Angew. Chem., Int. Ed.*, 2003, **42**, 3671–3673; (*c*) M. S. Seo, T. Kamachi, T. Kouno, K. Murata, M. J. Park, K. Yoshizawa and W. Nam, *Angew. Chem., Int. Ed.*, 2007, **46**, 2291–2294; (*d*) M. P. Jensen, A. M. i Payeras, A. T. Fiedler, M. Costas, J. Kaizer, A. Stubna, E. Münck and L. Que, Jr, *Inorg. Chem.*, 2007, **46**, 2398–2408.

5 (*a*) M. K. Coggins and J. A. Kovacs, *J. Am. Chem. Soc.*, 2011, **133**, 12470–12473; (*b*) M. K. Coggins, V. Martin-Diaconescu, S. DeBeer and J. A. Kovacs, *J. Am. Chem. Soc.*, 2013, **135**, 4260–4272.

6 (*a*) F. E. Jenney, Jr, M. F. J. M. Verhagen, X. Cui and M. W. W. Adams, *Science*, 1999, **286**, 306–309; (*b*) D. A. Kurtz, Jr, *Acc. Chem. Res.*, 2004, **37**, 902–908.

7 (*a*) J. A. Kovacs, *Chem. Rev.*, 2004, **104**, 825–848; (*b*) J. A. Kovacs and L. M. Brines, *Acc. Chem. Res.*, 2007, **40**, 501–509; (*c*) J. Shearer, R. C. Scarrow and J. A. Kovacs, *J. Am. Chem. Soc.*, 2002, **124**, 11709–11717; (*d*) T. Kitagawa, A. Dey, P. Lugo-Mas, J. B. Benedict, W. Kaminsky, E. I. Solomon and J. A. Kovacs, *J. Am. Chem. Soc.*, 2006, **128**, 14448–14449; (*e*) E. Nam, P. E. Alokolaro, R. D. Swartz, M. C. Gleaves, J. Pikul and J. A. Kovacs, *Inorg. Chem.*, 2011, **50**, 1592–1602.

8 (*a*) D. Krishnamurthy, G. D. Kasper, F. Namuswe, W. D. Kerber, A. A. N. Sarjeant, P. Moënne-Loccoz and D. P. Goldberg, *J. Am. Chem. Soc.*, 2006, **128**, 14222–14223; (*b*) F. Namuswe, G. D. Kasper, A. A. N. Sarjeant, T. Hayashi, C. M. Krest, M. T. Green, P. Moënne-Loccoz and D. P. Goldberg, *J. Am. Chem. Soc.*, 2008, **130**, 14189–14200; (*c*) F. Namuswe, T. Hayashi, Y. Jiang, G. D. Kasper, A. A. N. Sarjeant, P. Moënne-Loccoz and D. P. Goldberg, *J. Am. Chem. Soc.*, 2010, **132**, 157–167.

9 (*a*) A. Dey and E. I. Solomon, *Inorg. Chim. Acta*, 2010, **363**, 2762–2767; (*b*) A. Franke, C. Feritinger and R. van Eldik, *Chem.–Eur. J.*, 2012, **18**, 6935–6949.

10 (*a*) N. Lehnert, R. Y. N. Ho, L. Que, Jr and E. I. Solomon, *J. Am. Chem. Soc.*, 2001, **123**, 8271–8290; (*b*) N. Lehnert, R. Y. N. Ho, L. Que, Jr and E. I. Solomon, *J. Am. Chem. Soc.*, 2001, **123**, 12802–12816.

11 (*a*) Y. Zang, J. Kim, Y. Dong, E. C. Wilkinson, E. H. Appelman and L. Que, Jr, *J. Am. Chem. Soc.*, 1997, **119**, 4197–4205; (*b*) A. Wada, S. Ogo, Y. Watanabe, M. Mukai, T. Kitagawa, K. Jitsukawa, H. Masuda and H. Einaga, *Inorg. Chem.*, 1999, **38**, 3592–3593; (*c*) A. Wada, S. Ogo, S. Nagatomo, T. Kitagawa, Y. Watanabe, K. Jitsukawa and H. Masuda, *Inorg. Chem.*, 2002, **41**, 616–618; (*d*) M. R. Bukowski, H. L. Halfen, T. A. van den Berg, J. A. Halfen and L. Que, Jr, *Angew. Chem., Int. Ed.*, 2005, **44**, 584–587; (*e*) J. Bautz, P. Comba and L. Que, Jr, *Inorg. Chem.*, 2006, **45**, 7077–7082; (*f*) X. Shan, J.-U. Rohde, K. D. Koehntop, Y. Zhou, M. R. Bukowski, M. Costas, K. Fujisawa and L. Que, Jr, *Inorg. Chem.*, 2007, **46**, 8410–8417; (*g*) S. Gosiewska, H. P. Permentier, A. P. Bruins, G. van Koten and R. J. M. Klein Gebbink, *Dalton Trans.*, 2007, 3365–3368.

12 (*a*) E. K. Barefield, *Coord. Chem. Rev.*, 2010, **254**, 1607–1627; (*b*) J. Cho, R. Sarangi and W. Nam, *Acc. Chem. Res.*, 2012, **45**, 1321–1330.

13 S. Hong, H. So, H. Yoon, K.-B. Cho, Y.-M. Lee, S. Fukuzumi and W. Nam, *Dalton Trans.*, 2013, **42**, 7842–7845.

14 J.-J. Girerd, F. Banse and A. J. Simaan, *Struct. Bonding*, 2000, **97**, 145–177.

15 (*a*) C. V. Sastri, M. J. Park, T. Ohta, T. A. Jackson, A. Stubna, M. S. Seo, J. Lee, J. Kim, T. Kitagawa, E. Münck, L. Que, Jr and W. Nam, *J. Am. Chem. Soc.*, 2005, **127**, 12494–12495; (*b*) C. V. Sastri, J. Lee, K. Oh, Y. J. Lee, J. Lee, T. A. Jackson, K. Ray, H. Hirao, W. Shin, J. A. Halfen, J. Kim, L. Que, Jr, S. Shaik and W. Nam, *Proc. Natl. Acad. Sci. U. S. A.*, 2007, **104**, 19181–19186; (*c*) T. A. Jackson, J.-U. Rohde, M. S. Seo, C. V. Sastri, R. DeHont, A. Stubna, T. Ohta, T. Kitagawa, E. Münck, W. Nam and L. Que, Jr, *J. Am. Chem. Soc.*, 2008, **130**, 12394–12407; (*d*) S. A. Wilson, J. Chen, S. Hong, Y.-M. Lee, M. Clemancey, R. Garcia-Serres, T. Nomura, T. Ogura, J.-M. Latour, B. Hedman, K. O. Hodgson, W. Nam and E. I. Solomon, *J. Am. Chem. Soc.*, 2012, **134**, 11791–11806.

16 (*a*) S. P. de Visser, J.-U. Rohde, Y.-M. Lee, J. Cho and W. Nam, *Coord. Chem. Rev.*, 2013, **257**, 381–393; (*b*) A. R. McDonald and L. Que, Jr, *Coord. Chem. Rev.*, 2013, **257**, 414–428; (*c*) W. Nam, *Acc. Chem. Res.*, 2007, **40**, 522–531.

17 $[Fe^{II}(13\text{-TMC})(NCS)](CF_3SO_3)$ was synthesized as an authentic compound and its spectroscopic and structural characterizations were carried out (see ESI,† Fig. S7 for ESI MS and EPR spectra and Fig. S8 and Tables S2 and S3). X-ray crystal structure of $[Fe^{II}(13\text{-TMC})(NCS)](CF_3SO_3)$ clearly indicates that the N-donor of thiocyanate is coordinated to the $Fe^{II}$ centre.

18 This species is identified as $[Fe^{II}(13\text{-TMC})(NCS)]^+$ based on the ESI MS measurement of the reaction solution. The ESI MS clearly shows the presence of $[Fe^{II}(13\text{-TMC})(NCS)]^+$, not **1** (data not shown).
19 W. Kohn and L. J. Sham, *Phys. Rev.*, 1965, **140**, A1133–A1138.
20 DFT optimized structures were obtained based on the X-ray crystal structure of $[Fe^{II}(13\text{-TMC})(NCS)](CF_3SO_3)$ (see ref. 17).
21 (*a*) An octahedral iron(III) complex bearing an *N*-tetrametylated cyclam ligand is shown to contain high-spin Fe(III) ($S = 5/2$): J. F. Berry, E. Bill, R. Garcia-Serres, F. Neese, T. Weyhermüller and K. Wieghardt, *Inorg. Chem.*, 2006, **45**, 2027–2037; (*b*) Our DFT calculations indicate that the $NCS^-$ binding is endothermic by 10.8 kcal $mol^{-1}$, providing an explanation for its instability.
22 (*a*) D. V. Avila, C. E. Brown, K. U. Ingold and J. Lusztyk, *J. Am. Chem. Soc.*, 1993, **115**, 466–470; (*b*) M. Costas, K. Chen and L. Que, Jr, *Coord. Chem. Rev.*, 2000, **200–202**, 517–544; (*c*) E. Baciocchi, M. Bietti, M. Salamone and S. Stteenken, *J. Org. Chem.*, 2002, **67**, 2266–2270; (*d*) T. Tano, H. Sugimoto, N. Fujieda and S. Itoh, *Eur. J. Inorg. Chem.*, 2012, 4099–4103.
23 (*a*) S. Yoshioka, S. Takahashi, K. Ishimori and I. Morishima, *J. Inorg. Biochem.*, 2000, **81**, 141–151; (*b*) D. L. Harris and G. H. Loew, *J. Am. Chem. Soc.*, 1998, **120**, 8941–8948; (*c*) M. Sono, M. P. Roach, E. D. Coulter and J. H. Dawson, *Chem. Rev.*, 1996, **96**, 2841–2887; (*d*) T. L. Poulos, *J. Biol. Inorg. Chem.*, 1996, **1**, 356–359; (*e*) D. B. Goodin, *J. Biol. Inorg. Chem.*, 1996, **1**, 360–363; (*f*) J. H. Dawson, *Science*, 1988, **240**, 433–439.
24 (*a*) N. Hessenauer-Ilicheva, A. Franke, D. Meyer, W.-D. Woggon and R. van eldik, *Chem.–Eur. J.*, 2009, **15**, 2941–2959; (*b*) W. Nam, H. J. Han, S.-Y. Oh, Y. J. Lee, M.-H. Choi, S.-Y. Han, C. Kim, S. K. Woo and W. Shin, *J. Am. Chem. Soc.*, 2000, **122**, 8677–8684; (*c*) T. Matsui, S. Ozaki and Y. Watanabe, *J. Am. Chem. Soc.*, 1999, **121**, 9952–9957; (*d*) W. Nam, H. J. Choi, H. J. Han, S. H. Cho, H. J. Lee and S.-Y. Han, *Chem. Commun.*, 1999, 387–388; (*e*) F. Minisci, F. Fontana, S. Araneo, F. Recupero, S. Banfi and S. Quici, *J. Am. Chem. Soc.*, 1995, **117**, 226–232.
25 (*a*) M. D. Clay, F. E. Jenney, Jr, P. L. Hagedoorn, G. N. George, M. W. W. Adams and M. K. Johnson, *J. Am. Chem. Soc.*, 2002, **124**, 788–805; (*b*) R. Silaghi-Dumitrescu, I. Silaghi-Dumitrescu, E. D. Coulter and D. M. Kurtz, Jr, *Inorg. Chem.*, 2003, **42**, 446–456.
26 L. V. Liu, S. Hong, J. Cho, W. Nam and E. I. Solomon, *J. Am. Chem. Soc.*, 2013, **135**, 3286–3299.